# Journal of Materials Chemistry A

Accepted Manuscript






ROYAL SOCIETY OF CHEMISTRY

www.rsc.org/materialsA

Journal Name

COMMUNICATION

# Ultralight, compressible and multifunctional carbon aerogels based on natural tubular cellulose

Received 00th January 20xx,
Accepted 00th January 20xx

DOI: 10.1039/x0xx00000x

www.rsc.org/

Junping Zhang,[*a] Bucheng Li,[a] Lingxiao Li,[ab] and Aiqin Wang[a]

Ultralight, compressible and multifunctional carbon aerogels (UCM aerogels) have broad potential applications in various fields including thermal insulation, oil absorption and electronics. However, preparation of UCM aerogels has been proven very challenging. Herein, we report a novel approach for the fabrication of UCM aerogels by pyrolysis of aerogels composed of kapok fibers (KFs), a kind of natural cellulose with tubular structure. Different from the frequently used freeze-drying approach, the wet KFs aerogels can be dried directly in an oven without any shrinkage. The fascinating UCM aerogels feature ultralow density (~1.0 mg $cm^{-3}$), high compressibility, high electrical conductivity (0.1 S $cm^{-1}$), excellent fire-resistance and very high absorption capacity (147 ~ 292 g $g^{-1}$) for organic liquids. Furthermore, the UCM aerogels can be easily endowed with various other functions, e.g., magnetic responsivity and superhydrophobicity. The successful creation of the UCM aerogels may provide new insights into the design of UCM aerogels for various applications, as the UCM aerogels can be prepared via a very simple procedure.

Carbon aerogels are of great interest in various fields including thermal insulation, oil absorption, battery anodes and supercapacitors because of their unique properties such as low density, low thermal conductivity and high electrical conductivity, etc.[1-4] In recent years, cellular carbon aerogels with different properties and functionalities have been created by the assembly of various building blocks such as graphene,[5-10] carbon nanotubes (CNTs),[11] biomass (e.g., nanocellulose,[12] cotton[13] and watermelon[14]), glucose[15] and their combination,[16-18] etc. Freeze-drying of hydrogels,[16, 19] chemical vapor deposition[20] and template method[8, 21-23] are the frequently used strategies for the preparation of carbon aerogels. Although various novel carbon aerogels have been successfully prepared, practical applications of carbon aerogels have been hampered by the laborious strategies, expensive precursors and complex equipment. For example, the frequently used freeze-drying method for the preparation of carbon aerogels is time-consuming and energy-guzzling. In addition, the production of CNTs and graphene in bulk quantities is challenging. Moreover, the preparation of graphene oxide generates a large amount of acidic waste.

Natural materials like cellulose, starch and chitosan are receiving increasing attention in the preparation of functional materials due to their low cost, good availability and environmental benefits.[24, 25] Cellulose is one of the most important building blocks for the preparation of carbon aerogels.[26] Carbon aerogels with excellent properties have been prepared using nanocellulose[12] and bacterial cellulose[1] via freeze-drying. However, the strategies are still complicated and expensive. To address these problems, Zhang *et al*. prepared carbon aerogels by pyrolyzation of raw cotton and waste paper, which can be used as efficient and recyclable sorbents for oils and organic solvents.[13, 27] Nevertheless, the carbon aerogels based on raw cellulose and waste paper are not compressible and conductive. Compressible and multifunctional carbon aerogels from cellulose remained to be developed. All these issues push us to explore an efficient and economical strategy for preparation of multifunctional carbon aerogels with excellent elasticity.

The properties and functionalities of aerogels depend on both the properties of building blocks and the preparation strategies.[28-30] Herein, we report a very simple approach for the fabrication of ultralight, compressible and multifunctional carbon aerogels (UCM aerogels) based on a kind of natural tubular cellulose, kapok fibers (KFs, Fig. S1a). KFs are the seed hairs of the kapok tree (*Ceiba pentandra*) and are a typical cellulosic fiber with the features of thin cell wall, large lumen, low density and hydrophobic properties.[31] The UCM aerogels were prepared simply by activation of KFs with sodium chlorite (SC), filtration to yield the SC-KFs aerogels with diverse shapes, and then pyrolysis at 1000 °C in an $N_2$ atmosphere (Fig. 1a). Compared with the previously reported carbon aerogels, the UCM aerogels obtained in this study have the following advantages. (1) The UCM aerogels are prepared using natural cellulose with a tubular microstructure via a very simple strategy without freeze-drying and supercritical drying. (2) The UCM aerogels feature ultralow density, high compressibility, high electrical conductivity, excellent fire-resistance and very high absorption capacity for organic liquids. (3) The UCM aerogels can be further endowed with various other functions, e.g., magnetic responsivity and superhydrophobicity, via facile approaches.

[a] *Center of Eco-material and Green Chemistry and State Key Laboratory for Oxo Synthesis & Selective Oxidation, Lanzhou Institute of Chemical Physics, Chinese Academy of Sciences, 730000, Lanzhou, P.R. China. E-mail: jpzhang@licp.cas.cn*
[b] *Graduate University of the Chinese Academy of Sciences, 100049, Beijing, P. R. China.*

† Electronic Supplementary Information (ESI) available: [Experimental Section, SEM images, XPS, TGA and DSC analyses, variation of density, conductivity and compressibility as well as videos]. See DOI: 10.1039/x0xx00000x

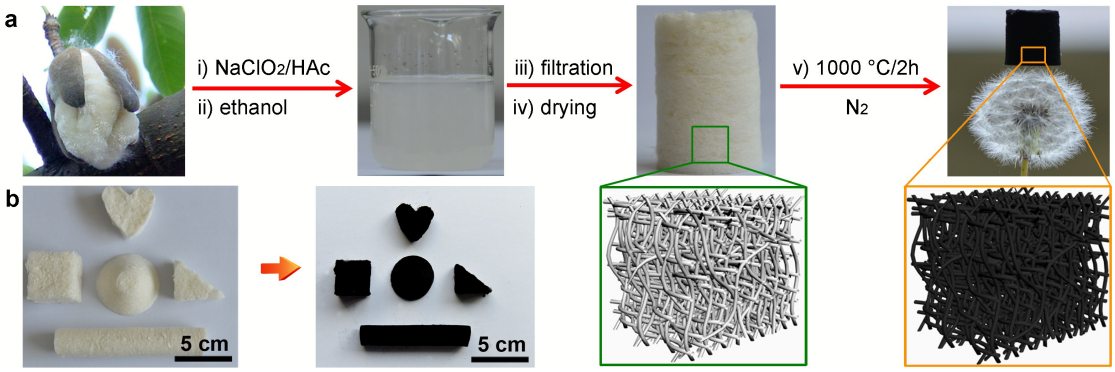


**Fig. 1** (a) Preparation of the UCM aerogels, and (b) optical images of the SC-KFs and the corresponding UCM aerogels with diverse shapes.

Fig. 1a describes the strategy for the preparation of the UCM aerogels. KFs were treated in a SC aqueous solution in the presence of acetic acid at 80 °C, and then homogenized to form well-dispersed SC-KFs in ethanol. Subsequently, the SC-KFs in ethanol were readily filtered to yield the wet SC-KFs aerogels with diverse shapes (e.g., cylinder, cube, cone and the heart-shaped one), directly dried in an oven at 60 °C, and then pyrolyzed at 1000 °C in an $N_2$ atmosphere for a period of time. It should be noted that the KFs cannot be used directly for preparation of the UCM aerogels and SC treatment is necessary in order to keep the shape of the SC-KFs aerogels after drying. Different from the frequently used freeze-drying and supercritical drying approaches, the wet SC-KFs aerogels with absorbed ethanol can be dried directly in an oven. No shrinkage of the SC-KFs aerogels was observed in the drying process (Fig. S2). This is because the aerogel is macroscopically rough and is composed of SC-KFs with the micro-tubular structure. This is different from the aerogels based on nano building blocks such as graphene, carbon nanotubes and nanocellulose, etc. Both the macroscopically rough topography and the micro-tubular structure of the wet SC-KFs aerogel are convenient for the evaporation of the absorbed ethanol. The low surface tension and the high volatility of ethanol should also be responsible for the phenomenon. After pyrolysis under the optimal conditions, the black UCM aerogels with a density of as low as 1 mg $cm^{-3}$ were successfully fabricated. The volume of the UCM aerogels is ~36% of that of the SC-KFs aerogel (Fig. 1b).

The porous SC-KFs aerogel is composed of interpenetrated tubular fibers (Fig. S1b). The fibers are ~20 μm in diameter and several millimeters in length. The SC treatment has no influence on surface morphology and tubular structure of KFs (Fig. S3a-b). In contrast, the fibers in the UCM aerogel are still intact but partly become flat (Figs. 2a and S3c), which is consistent with the volume shrinkage in the pyrolysis process. No apparent difference in morphology was observed from the UCM aerogels generated at different temperature (Fig. S4). The X-ray diffraction (XRD) patterns of KFs and SC-KFs showed two peaks at 15.49° and 22.12°, corresponding to the typical (110) and (020) planes of cellulose, respectively (Fig. 2b).[1] After pyrolysis at 400 ~ 1000 °C, the peak at 15.49° disappeared and the peak at 22.12° became broad, indicating that the crystalline structure of KFs was destroyed and amorphous carbon was formed.

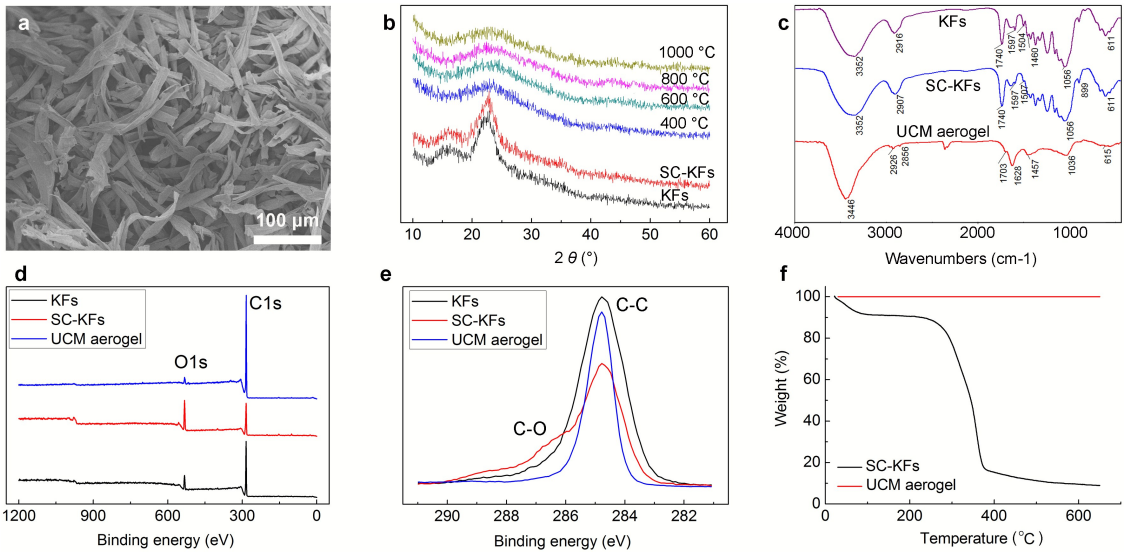


**Fig. 2** (a) SEM image of the UCM aerogel, (b) XRD patterns of KFs, SC-KFs and the UCM aerogels pyrolyzed at different temperature, (c) FTIR spectra, (d) XPS spectra, (e) high-resolution C 1s spectra and (f) TGA curves of KFs, SC-KFs and the UCM aerogel (1000 °C, 2 h) in an $N_2$ atmosphere.

The effects of SC treatment and pyrolysis were also studied by Fourier transformed infrared (FTIR) spectroscopy (Fig. 2c). KFs contain many functional groups, such as -OH (3352 $cm^{-1}$), C-H (2916 $cm^{-1}$), C=O (1740 $cm^{-1}$) and C-O (1056 $cm^{-1}$). The SC treatment removed wax on the surface of KFs, broke a part of hydrogen bonding and oxidated lignin in KFs (see Supporting Information for detailed discussion).[32] These functional groups became weak or disappeared after pyrolysis at 1000 °C, indicating carbonization of KFs. The results were further confirmed by X-ray photoelectron spectroscopy (XPS) analysis (Fig. 2d-e, Fig. S5 and Table S1). After SC treatment, the O/C atomic ratio increased from 0.12 to 0.31 because of removal of wax on the surface of KFs and formation of carbonyl species. The O/C atomic ratio decreased to 0.04 after pyrolysis at 1000 °C. The weight loss of SC-KFs in the pyrolysis process was investigated by thermal gravimetric analysis (TGA, Figs. 2f and S6). SC-KFs showed evident weight loss (~80%) in the temperature range of 280 °C to 520 °C. The weight of the residue is ~9.5% of that of SC-KFs and ~8% of that of KFs. No weight loss of the UCM aerogel was observed until 650 °C, as the aerogel was prepared by pyrolysis of SC-KFs at 1000 °C in an $N_2$ atmosphere.

Pyrolysis condition has great influences on the products and their properties. It was found that the pyrolysis temperature and pyrolysis time have great influences on density, conductivity and elasticity of the UCM aerogels. With increasing the pyrolysis temperature to 1000 °C, the volume shrinkage of the aerogel increased to 64% and the density of the UCM aerogel decreased linearly to ~1.0 mg $cm^{-3}$ (Figs. S7 and S8), which is consistent with the TGA result. Meanwhile, the aerogel became conductive at temperature higher than 800 °C. Moreover, a higher pyrolysis temperature evidently improved compressibility of the UCM aerogel (Fig. S9). After one cycle of 80% compressive strain, the aerogel prepared at 400 °C can only recover 51.4% of its original volume, whereas that prepared at 1000 °C can recover 92.6% of its original volume. Similarly, a longer pyrolysis time at 1000 °C decreased density and improved elasticity of the aerogels (Figs. S10 and S11). However, a pyrolysis time of longer than 2 h resulted in decrease of the conductivity.

The UCM aerogel prepared under the optimal condition has a ultralow density of 1~2 mg $cm^{-3}$, which is lower than many of the aerogels based on silicone, cellulose, CNTs and graphene,[6, 11, 29, 33-35] comparable to some of the aerogels based on CNTs, graphene and biomass, etc.[1, 21, 27, 36, 37] The density of the UCM aerogel is only slightly larger than the ultra-flyweight CNTs/graphene aerogel (0.75 mg $cm^{-3}$) and the FIBER aerogel (0.12 mg $cm^{-3}$) (Table S2).[16] A piece of the UCM aerogel can stand stably on top of a dandelion and no deformation of the dandelion was observed (Fig. 1a).

Interestingly, the UCM aerogel is compliant with excellent compressive properties, which is rare for cellulose-based aerogels, e.g., the carbon fiber aerogels made from raw cotton by Zhang et al.[5] The UCM aerogel can withstand a compressive strain of as high as 80% and almost recover its original shape after release of the stress as shown in Fig. 3a. The successive cyclic compressive stress-strain curves of the UCM aerogel with different strain (40%, 60% and 80%) are shown in Fig. 3b. The compressive stress increased gradually with the strain when the strain was less than 60% (linear elastic regime) because of elastic bending of the fibers.[1, 38] The compressive stress increased steeply with further increasing the strain to 80% (densification regime) because of impinging among the fibers. The UCM aerogel can even bear the successive cyclic compression test with 1000 loading-unloading cycles at 60% strain (Fig. 3c). No fracture or collapse of the aerogel was observed during the test. The UCM aerogel exhibited only 10.6% deformation at the 100th cycle and 15.3% deformation at the 1000th cycle, demonstrating excellent compressibility. The deformation of the UCM aerogel in the cyclic compression test is lower than many of the polymeric foams and fibrous aerogels.[39] In addition, no significant decrease in the maximum stress was observed during the test. The UCM aerogel retained over 72% of its original stress after

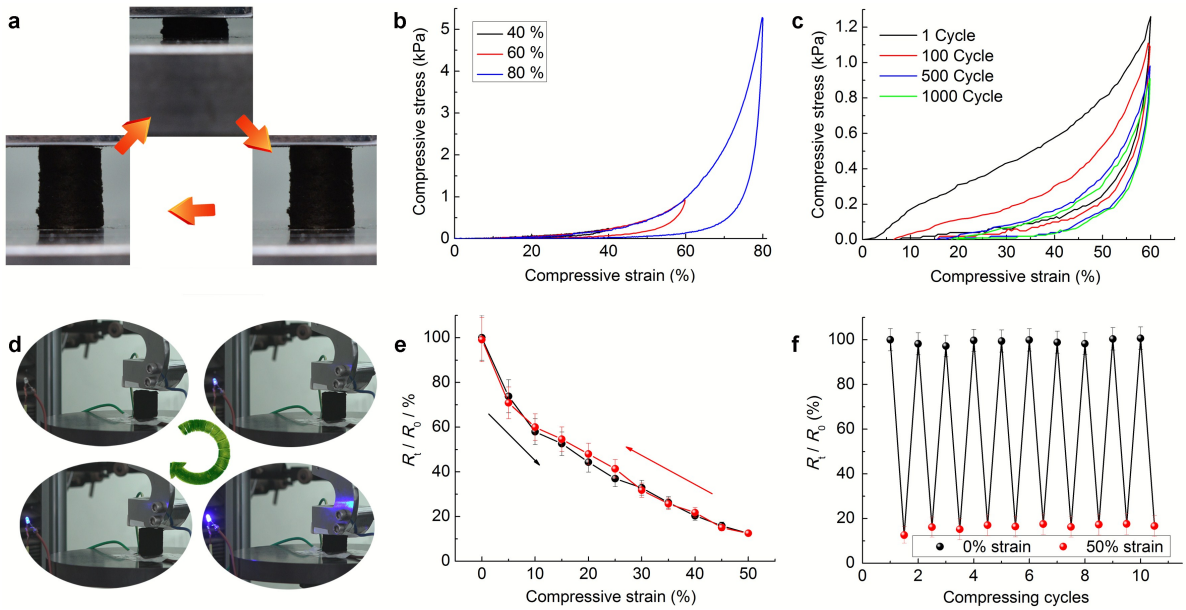


**Fig. 3** (a) Reversible compression of the UCM aerogel, compressive stress-strain curves of the UCM aerogel with different (b) strain and (c) cycles, (d) strain-controlled on-off of a light-emitting diode using the UCM aerogel, (e) variation of $R_t/R_0$ of the UCM aerogel with compressive strain in one cycle and (f) variation of $R_t/R_0$ of the UCM aerogel with repeatedly compressive strain (50%) for 10 cycles.

1000 cycles at 60% strain. The robust compressibility of the UCM aerogel is attributed to both the tubular structure of the fibers and the network formed by the interpenetrated fibers.

Besides ultralow density and excellent compressive properties, the UCM aerogel is also conductive with a conductivity of 0.10 S $cm^{-1}$. Thus, the UCM aerogel exhibited strain-dependent electrical conductivity owing to the combination of compressibility and conductivity. A light-emitting diode was illumined when linked to a circuit using the UCM aerogel. The brightness of the diode changed with compressive strain of the UCM aerogel (Fig. 3d and Movie S1). The conductivity of the UCM aerogel is very sensitive to strain of the UCM aerogel. The normalized electrical resistance ($R_t/R_0$) of the aerogel decreased nearly linearly to 87.5% with increasing the strain to 50% and recovered very well after release of the stress (Fig. 3e). This is because more contacting points among the fibers are formed due to elastic bending of the fibers during compression of the aerogel, which resulted in decrease of the electrical resistance. The sensitivity of $R_t/R_0$ of the UCM aerogel to compressive strain is higher than many of the previously reported conductive aerogels. Furthermore, the response of $R_t/R_0$ to compressive strain is quite stable over 10 compressing cycles (Fig. 3f), which is attributed to excellent compressibility of the UCM aerogel. The high sensitivity and reversibility of the UCM aerogel make it a very promising pressure-sensitive material, and may find applications in various fields such as sensors and electronics.

The UCM aerogel is hydrophobic/superoleophilic with a water contact angle of 140.2° and an oil contact angle of 0°, which endows it with high selectivity for absorbing organic pollutants and oils from water. In addition, the porous skeleton of the UCM aerogel and the tubular structure of the KFs provide a large volume for the storage of absorbed liquids. The UCM aerogel can be used for selective absorption of floating oils on water surface (Fig. 4a-i and Movie S2, part 1) and heavy oils under water (Fig. 4a-ii) within a few seconds. The oil-loaded aerogels remained floating on water surface because of its ultralow density and can be easily taken out of water after complete absorption of oils, resulting in the cleaned water. The UCM aerogel can also be used as a membrane for oil/water separation (Fig. 4a-iii and Movie S2, part 2). Once an oil/water mixture was poured into the custom built setup, oils were quickly absorbed by the aerogel or penetrated the aerogel and dropped into the bottle beneath it. Meanwhile, more and more water was collected on the surface of the aerogel. After absorption equilibrium, the absorbed oil must be collected from the aerogel in order to be used for the next cycle. For expanding its practical applicability in the continuous collecting of a large amount of oil from water, the UCM aerogel was fixed at the opening of a tube and combined with a pump (Fig. 4a-iv and Movie S2, part 3-4). Once the pump was started, the absorbed oil in the aerogel can be pumped into the collector through the tube and the released space in the aerogel can absorb the excess oil on water surface. Thus, the absorption and collection of oil can be achieved simultaneously and continuously. A large volume of oil could be successfully collected using a small piece of the UCM aerogel with the help of a pump.

The UCM aerogel showed very high absorption capacity for various frequently encountered organic liquids including fuels, alkanes, chloroalkanes and aromatic compounds (Fig. 4b). The absorption capacity of the UCM aerogel for these organics is in the range of 147 to 292 g $g^{-1}$ depending on density of the organics. For example, the absorption capacity of the aerogel for *n*-hexane (density = 0.66 g $cm^{-3}$) is 169 g $g^{-1}$ and for tetrachloromethane (density = 1.60 g $cm^{-3}$) is 292 g $g^{-1}$. The absorption capacity of the UCM aerogel is much higher than many previously reported

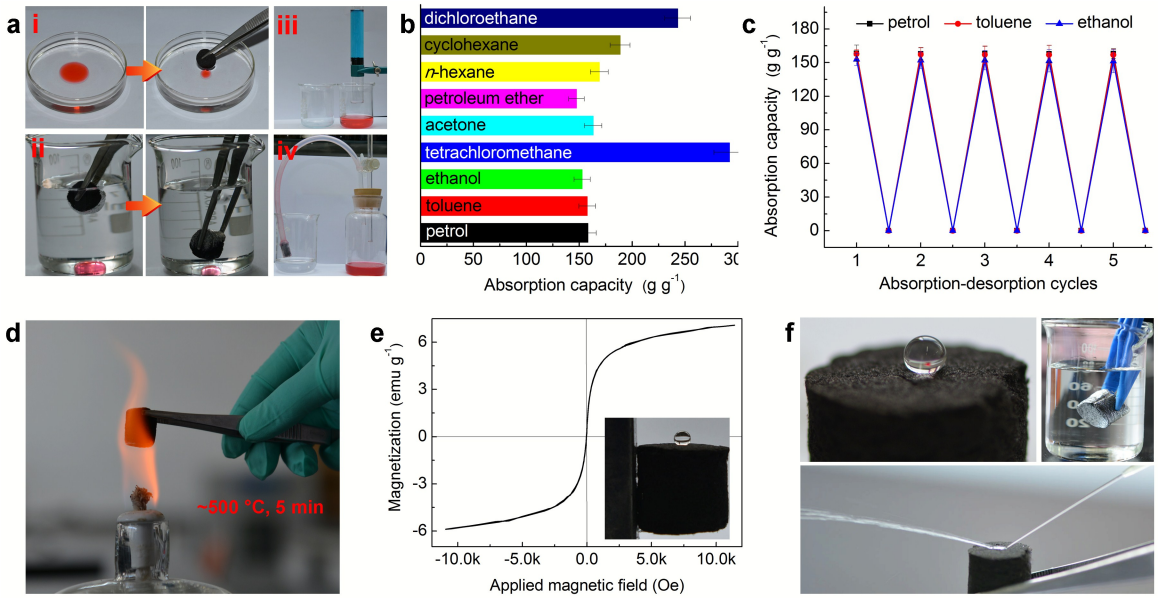


**Fig. 4** (a) Oil/water separation using the UCM aerogel with a density of 2 mg $cm^{-3}$ and a weight of ~10 mg via various approaches (i. absorption of floating oil, ii. absorption of heavy oil under water, iii. oil/water separation, iv. pump-assisted continuous oil absorption), (b) absorption capacity of the UCM aerogel for different organics, (c) variation of absorption capacity with absorption-desorption cycles, (d) flame retardency of the UCM aerogel, (e) magnetic curve (300 K) of the UCM/$Fe_3O_4$ aerogel and (f) superhydrophobicity of the UCM@PDMS aerogels. Water was colored with methylene blue and oils were colored with oil red O. The inset in (e) showed the UCM/$Fe_3O_4$ aerogel with a water droplet (7 μL) lifted by a magnet.

absorbents (Table S3), such as superhydrophobic polyurethane sponges (13~45 g $g^{-1}$),[40-42] silicone sponges (6~18 g $g^{-1}$),[33, 43] graphene sponges (20~86 g $g^{-1}$),[44] CNTs sponges (88~170 g $g^{-1}$)[11] and carbon aerogels (40~192 g $g^{-1}$).[13, 21, 22, 27] Although the absorption capacity of the UCM aerogel is comparable to the carbon nanofiber aerogels from bacterial cellulose (106~312 g $g^{-1}$)[1] and still lower than the ultra-flyweight CNTs/graphene aerogel,[16] the UCM aerogel has remarkable superiorities including very simple preparation method and very cheap building blocks among all these absorbents. In addition, no dripping of the absorbed liquids was observed in the handling process indicating firm absorption by the aerogel. Moreover, the UCM aerogel can be repeatedly used for the absorption of various oils (Fig. 4c). The increase in the absorption cycles almost has no influence on the absorption capacity, which is attributed to the inherent stability of the aerogel towards organic liquids. Furthermore, the UCM aerogel exhibits excellent fire resistance (Fig. 4d). The UCM aerogel does not show any burning or changes in shape, size and porous structure even after exposed to the flame of a spirit lamp (~500 °C) for 5 min as shown in Movie S3. The very high absorption capacity, excellent reusability and fire resistance of the UCM aerogel ensure its application for the cleanup of oils from water.

We have tried to prepare UCM aerogels using the other biomass fibers such as cotton and wastepaper. It was found that aerogels could be successfully obtained via the same strategy using wastepaper. The optimal condition is different from that of the KFs, and we will study it later. However, it is difficult to make the cotton fibers disperse uniformly in ethanol because the cotton fibers are very long compared to KFs. We have tried to shorten the cotton fibers using a shredding machine but failed. We expect that aerogels based on cotton fibers could also be obtained if the fibers can be shortened via a proper method.

The UCM aerogels can be further endowed with various other functions, e.g., magnetic responsivity and superhydrophobicity, via facile approaches. Magnetic UCM/$Fe_3O_4$ aerogels with a saturation magnetization of 7.1 emu $g^{-1}$ at 300 K were synthesized by incorporating $Fe_3O_4$ nanoparticles (8-16 nm) into the network of the UCM aerogels via a dip-coating method. The magnetic UCM/$Fe_3O_4$ aerogels keep the porous structure of the UCM aerogels (Fig. S12). The $Fe_3O_4$ nanoparticles distributed uniformly on the surface of the fibers and slightly increased the weight of the UCM aerogels by 2-5%. The UCM/$Fe_3O_4$ aerogel shows standard paramagnetic characteristic curve with no hysteresis after removal of the magnetic field (Fig. 4e). A piece of the UCM/$Fe_3O_4$ aerogel (density = 3.2 ± 0.3 mg $cm^{-3}$) with a water droplet (7 μL) could be lifted by a magnet (inset in Fig. 4e). Superhydrophobic UCM@PDMS aerogels were prepared by chemical vapor deposition of PDMS at 180 °C on the surface of the fibers in the UCM aerogels. Water drops showed a very high contact angle (156.6° ± 1.8°) on the UCM@PDMS aerogel and could easily roll off the slightly tilted (4° ± 1.0°) sample (Fig. 4f). Water drops on both the surface and the cross section are spherical in shape, indicating uniformity of the superhydrophobic coating. In addition, when the aerogel was immersed in water by an external force, it was reflective because of existence of an air cushion between water and the aerogel, which means that water is in the Cassie-Baxter state, and the interaction between water and the UCM@PDMS aerogel is very weak. Interestingly, a jet of water from a pipette or a tap could bounce off the UCM@PDMS aerogel without leaving a trace, indicating excellent superhydrophobicity.

In summary, we have successfully developed a simple approach for the preparation of ultralight, compressible and multifunctional carbon aerogels based on natural tubular KFs. Different from the frequently used freeze-drying approach, the wet SC-KFs aerogels can be dried directly in an oven without any shrinkage. It was found that the pyrolysis temperature and pyrolysis time have great influences on density, conductivity and elasticity of the UCM aerogels. The UCM aerogels feature ultralow density, high compressibility, high electrical conductivity, excellent fire resistance and very high absorption capacity for organic liquids. Furthermore, the UCM aerogels can be endowed with various other functions, e.g., magnetic responsivity and superhydrophobicity, via facile approaches. Thus, the UCM aerogels may find applications in various fields such as sensors, pressure-sensitive electronics and cleanup of oils from water, etc.

## Acknowledgements

We are grateful for financial support of the "Hundred Talents Program" of the Chinese Academy of Sciences.

## Notes and references

1. Z. Y. Wu, C. Li, H. W. Liang, J. F. Chen and S. H. Yu, *Angew. Chem. Int. Ed.*, 2013, **52**, 2925-2929.
2. A. C. Pierre and G. M. Pajonk, *Chem. Rev.*, 2002, **102**, 4243-4266.
3. Z. S. Wu, S. Yang, Y. Sun, K. Parvez, X. Feng and K. Mullen, *J. Am. Chem. Soc.*, 2012, **134**, 9082-9085.
4. R. J. White, N. Brun, V. L. Budarin, J. H. Clark and M.-M. Titirici, *ChemSusChem*, 2014, **7**, 670-689.
5. V. Chabot, D. Higgins, A. P. Yu, X. C. Xiao, Z. W. Chen and J. J. Zhang, *Energy Environ. Sci.*, 2014, **7**, 1564-1596.
6. Z. Xu, Y. Zhang, P. Li and C. Gao, *ACS Nano*, 2012, **6**, 7103-7113.
7. H. Hu, Z. Zhao, W. Wan, Y. Gogotsi and J. Qiu, *Adv. Mater.*, 2013, **25**, 2219-2223.
8. C. Wu, X. Huang, X. Wu, R. Qian and P. Jiang, *Adv. Mater.*, 2013, **25**, 5658-5662.
9. X. Cao, Z. Yin and H. Zhang, *Energy Environ. Sci.*, 2014, **7**, 1850-1865.
10. J. Luo, J. Liu, Z. Zeng, C. F. Ng, L. Ma, H. Zhang, J. Lin, Z. Shen and H. J. Fan, *Nano Lett.*, 2013, **13**, 6136-6143.
11. X. Gui, J. Wei, K. Wang, A. Cao, H. Zhu, Y. Jia, Q. Shu and D. Wu, *Adv. Mater.*, 2010, **22**, 617-621.
12. M. Hamedi, E. Karabulut, A. Marais, A. Herland, G. Nyström and L. Wågberg, *Angew. Chem. Int. Ed.*, 2013, **52**, 12038-12042.
13. H. Bi, Z. Yin, X. Cao, X. Xie, C. Tan, X. Huang, B. Chen, F. Chen, Q. Yang, X. Bu, X. Lu, L. Sun and H. Zhang, *Adv. Mater.*, 2013, **25**, 5916-5921.
14. X. L. Wu, T. Wen, H. L. Guo, S. Yang, X. Wang and A. W. Xu, *ACS Nano*, 2013, **7**, 3589-3597.

15. T. P. Fellinger, R. J. White, M. M. Titirici and M. Antonietti, *Adv. Funct. Mater.*, 2012, **22**, 3254-3260.
16. H. Sun, Z. Xu and C. Gao, *Adv. Mater.*, 2013, **25**, 2554-2560.
17. B. Wicklein, A. Kocjan, G. Salazar-Alvarez, F. Carosio, G. Camino, M. Antonietti and L. Bergström, *Nat. Nano.*, 2015, **10**, 277-283.
18. M. Wang, I. V. Anoshkin, A. G. Nasibulin, J. T. Korhonen, J. Seitsonen, J. Pere, E. I. Kauppinen, R. H. A. Ras and O. Ikkala, *Adv. Mater.*, 2013, **25**, 2428-2432.
19. H. B. Yao, G. Huang, C. H. Cui, X. H. Wang and S. H. Yu, *Adv. Mater.*, 2011, **23**, 3643-3647.
20. E. Singh, Z. Chen, F. Houshmand, W. Ren, Y. Peles, H. M. Cheng and N. Koratkar, *Small*, 2013, **9**, 75-80.
21. H. W. Liang, Q. F. Guan, L. F. Chen, Z. Zhu, W. J. Zhang and S. H. Yu, *Angew. Chem. Int. Ed.*, 2012, **51**, 5101-5105.
22. N. Chen and Q. Pan, *ACS Nano*, 2013, **7**, 6875-6883.
23. H. Bi, I. W. Chen, T. Lin and F. Huang, *Adv. Mater.*, 2015, **27**, 5943-5949.
24. R. T. Olsson, M. A. S. Azizi Samir, G. Salazar Alvarez, L. Belova, V. Strom, L. A. Berglund, O. Ikkala, J. Nogues and U. W. Gedde, *Nat. Nano.*, 2010, **5**, 584-588.
25. B. Ghosh and M. W. Urban, *Science*, 2009, **323**, 1458-1460.
26. Z. Zhang, G. Sèbe, D. Rentsch, T. Zimmermann and P. Tingaut, *Chem. Mater.*, 2014, **26**, 2659-2668.
27. H. Bi, X. Huang, X. Wu, X. Cao, C. Tan, Z. Yin, X. Lu, L. Sun and H. Zhang, *Small*, 2014, **10**, 3544-3550.
28. M. Rousseas, A. P. Goldstein, W. Mickelson, M. A. Worsley, L. Woo and A. Zettl, *ACS Nano*, 2013, **7**, 8540-8546.
29. M. Kettunen, R. J. Silvennoinen, N. Houbenov, A. Nykänen, J. Ruokolainen, J. Sainio, V. Pore, M. Kemell, M. Ankerfors and T. Lindström, *Adv. Funct. Mater.*, 2011, **21**, 510-517.
30. Y. Qian, I. M. Ismail and A. Stein, *Carbon*, 2014, **68**, 221-231.
31. Y. Zheng, J. Wang, Y. Zhu and A. Wang, *J. Environ. Sci.*, 2015, **27**, 21-32.
32. J. P. Zhang, L. Wu, Y. J. Zhang and A. Q. Wang, *J. Mater. Chem. A*, 2015, **3**, 18475-18482.
33. L. Li, B. Li, L. Wu, X. Zhao and J. Zhang, *Chem. Commun.*, 2014, **50**, 7831-7833.
34. Q. Peng, Y. Li, X. He, X. Gui, Y. Shang, C. Wang, C. Wang, W. Zhao, S. Du, E. Shi, P. Li, D. Wu and A. Cao, *Adv. Mater.*, 2014, **26**, 3241-3247.
35. C. Zhu, T. Y. Han, E. B. Duoss, A. M. Golobic, J. D. Kuntz, C. M. Spadaccini and M. A. Worsley, *Nat. Commun.*, 2015, **6**, 6962.
36. J. Zou, J. Liu, A. S. Karakoti, A. Kumar, D. Joung, Q. Li, S. I. Khondaker, S. Seal and L. Zhai, *ACS Nano*, 2010, **4**, 7293-7302.
37. Y. Zhao, C. Hu, Y. Hu, H. Cheng, G. Shi and L. Qu, *Angew. Chem. Int. Ed.*, 2012, **124**, 11533-11537.
38. K. H. Kim, Y. Oh and M. F. Islam, *Nat. Nano.*, 2012, **7**, 562-566.
39. Y. Si, J. Yu, X. Tang, J. Ge and B. Ding, *Nat. Commun.*, 2014, **5**, 5802.
40. L. Wu, L. Li, B. Li, J. Zhang and A. Wang, *ACS Appl. Mater. Interfaces*, 2015, **7**, 4936-4946.
41. B. C. Li, L. X. Li, L. Wu, J. P. Zhang and A. Q. Wang, *ChemPlusChem*, 2014, **79**, 850-856.
42. Q. Zhu and Q. Pan, *ACS Nano*, 2014, **8**, 1402-1409.
43. G. Hayase, K. Kanamori, M. Fukuchi, H. Kaji and K. Nakanishi, *Angew. Chem. Int. Ed.*, 2013, **52**, 1986-1989.
44. H. Bi, X. Xie, K. Yin, Y. Zhou, S. Wan, L. He, F. Xu, F. Banhart, L. Sun and R. S. Ruoff, *Adv. Funct. Mater.*, 2012, **22**, 4421-4425.